


## Evaluation of hydrological responses to climate change for a data-scarce mountainous watershed in Taiwan

Yi-Hsuan Roger Chen<sup>a</sup>, Hung-Wei Tseng<sup>b</sup>, Kuo-Chin Hsu <sup>c,\*</sup>, Shang-Ying Chen<sup>c</sup>, Chien-Chung Ke<sup>d</sup> and Li-Chi Chiang<sup>e</sup>

<sup>a</sup> Department of Environmental Health and Engineering, Johns Hopkins University, Baltimore, MD, USA

<sup>b</sup> Department of Hydraulic and Ocean Engineering, National Cheng Kung University, 1 University Road, Tainan, Taiwan, R.O.C.

<sup>c</sup> Department of Resources Engineering, National Cheng Kung University, 1 University Road, Tainan, Taiwan, R.O.C.

<sup>d</sup> Geotechnical Engineering Research Center, Sinotech Engineering Consultants, Inc., 280 Xinhua 2nd Rd., Neihu Dist., Taipei, Taiwan, R.O.C.

<sup>e</sup> Department of Bioenvironmental System Engineering, National Taiwan University, 1, Section 4, Roosevelt Road, Taipei, Taiwan, R.O.C.

\*Corresponding author. E-mail: kchsu@mail.ncku.edu.tw

 K-CH, 0000-0002-1126-8008

### ABSTRACT

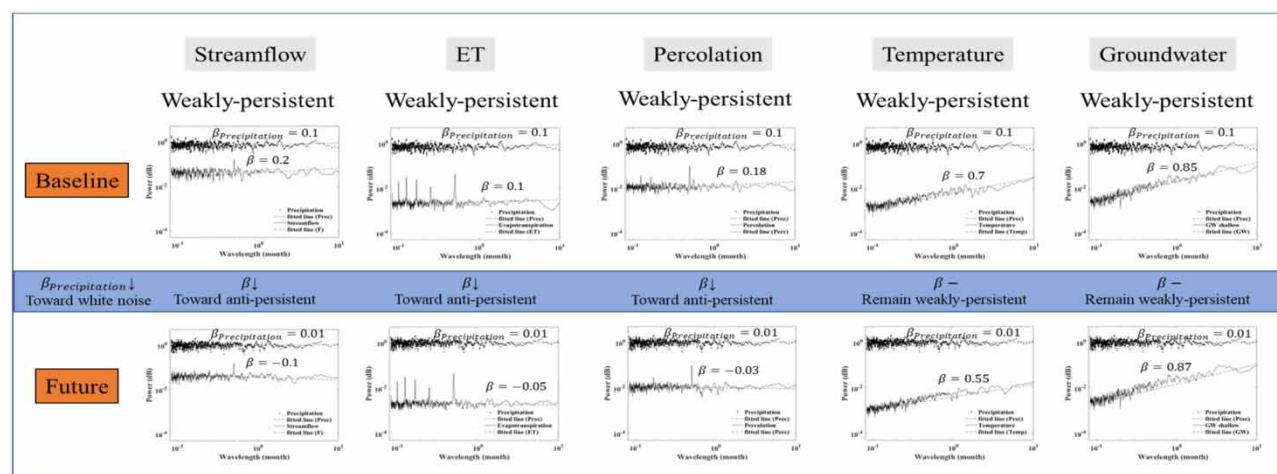
Despite the mountainous watersheds being important for the ecosystem, water resources, and hydropower, little hydrological data has been collected. This data scarcity makes it difficult to evaluate their hydrologic response to climate change. This study integrated short-term hydrological data with physics-based meteorological and hydrological models to measure the impact of climate change on future water scarcity in the Wuling Mountain Watershed, Taiwan. Twenty-eight-month hydrological datasets from 2013 to 2015 were used for the hydrological characterization. Scenarios from CMIP5 were selected for the climate projection for the period 2021–2040 based on the inferred 1986–2005 baseline data. The results showed that precipitation, water percolation, and streamflow will decrease by about 10% and increase by about 20–25% in the dry and wet seasons, respectively. The evapotranspiration is lower than that of the baseline in January, March, and December, whereas it can be as high as 4% during the other months. The increase in the annual amount and change in the water distribution for all studied water components indicate the possible acceleration of the water cycle. Spectrum analysis showed that surface water tends toward becoming more irregular. Groundwater remains mildly persistent and thus may serve as a buffer for the impact of climate change on water resources.

**Key words:** climate change, data-scarce watershed, fractal analysis, hydrological response, physical-based model

### HIGHLIGHTS

- Physics-based meteorological and hydrological models were integrated to evaluate hydrological responses to climate change for a data-scarce mountainous watershed.
- Changes in hydrological components indicate the acceleration and complication of the water cycle in the future.
- Surface water tends toward becoming more irregular and groundwater may serve as a buffer for the impact of climate change on water resources.

## GRAPHICAL ABSTRACT



Criteria:  $\beta > 1$ : strong persistence;  $1 > \beta > 0$ : weakly persistent;  $\beta = 0$ : uncorrelated;  $\beta < 0$ : anti-persistence

## INTRODUCTION

Improved living standards have resulted in a substantial increase in the human population; overall, this has resulted in a greater demand for various resources (i.e., food, energy, and water). For the proper management of water resources, predictive hydrological models are necessary to quantitatively map their dynamics (Tsegaw *et al.* 2020). However, global climate change poses challenges to managing water resources. Liu *et al.* (2016) showed that global trends in regional annual precipitation were primarily driven by the changes due to the top 30% of heavy precipitation events during the major global warming period from 1979 to 2013. Sharma *et al.* (2018) noted that the discharge in small catchments is highly sensitive to temperature. Due to the relatively smaller spatial range of catchments, storms tend to encompass an entire catchment, resulting in complete saturation of the soil, thereby impacting streamflow. Therefore, changes in precipitation and temperature can significantly impact hydrological responses, which may lead to potential disasters due to water resource scarcity (IPCC 2022).

Predicting the responses of a hydrological system to climate change is important within the context of effectively managing water resources. However, challenges in understanding the hydrological responses of watersheds to climate change are often caused by the complex interactions of the system components, different scales of hydrological processes, difficulty in accurately measuring hydrological components, and insufficient long-term hydrological records. Owing to the complex interactions of the natural and anthropogenic influences in the hydrological cycle, it is difficult to isolate individual factors that shape it. Thus, mountainous watersheds and rural areas are ideal for the exploration of natural hydrological responses to climate change; this is primarily due to the fact that most of them have experienced minimal anthropogenic interferences. However, data on mountainous watersheds are usually scarce or not comprehensive (Afshar *et al.* 2017). Nonetheless, hydrological analyses have been conducted on data-scarce watersheds (Huang & Yang 2015; Liang *et al.* 2015; Tegegne *et al.* 2017).

Hydrological analyses can be classified into two groups, namely, physics-based (knowledge-driven) models and data-driven (empirical) models (Zheng *et al.* 2018). Data-driven models have been widely used owing to their simplicity and flexibility (Sivakumar & Berndtsson 2010). Specifically, data-driven models, such as the unit hydrograph method, various statistical models (i.e., linear regression, multi-linear, and ARIMA), and machine learning models (Anaraki *et al.* 2020; Farzin & Anaraki 2021; Farzin *et al.* 2022; Kakhodazadeh *et al.* 2022), rely on a large amount of training data to describe the responses of the modeled system (Hurst 1951; Solomatine & Ostfeld 2008; Conoscenti *et al.* 2014; Taormina & Chau 2015; Pourghasemi *et al.* 2017; Bai *et al.* 2019). On the other hand, physics-based models are based on an understanding of system behavior (Zahabioun *et al.* 2013), and simulations of the hydrological responses are based on the first-order principles from the physics of a phenomenon or system (Liu *et al.* 2020). This type of model can be further subdivided, depending on the treatment of the system, into distributed or lumped models. Distributed models describe spatiotemporal hydrological

responses, whereas lumped models provide representative hydrological characteristics for the entire watershed. Distributed models are often used for rigorous hydrology modeling. To date, several well-developed distributed physics-based models have been developed, including GR4J (Perrin *et al.* 2003), HSPF (Borah & Bera 2003), and the soil and water assessment tool (SWAT) (Bieger *et al.* 2017). The advantages of using distributed physics-based models include their excellent forecasting ability and the successful modeling of detailed spatial information using limited hydrological data (Balica *et al.* 2013). Therefore, physics-based models may be preferred for watersheds with scarce data.

Spectral analysis is a powerful technique for measuring the persistence of hydrological time series (Zhou *et al.* 2020). Several studies have characterized the fractal behavior of hydrological responses through spectral analysis (Bai *et al.* 2019). The fractal phenomenon, found across various fields (López-Ortega *et al.* 2020), was first reported by Hurst (1951) during an investigation of the discharge time series of the Nile River within the design framework of the Aswan High Dam. Kirchner *et al.* (2000) showed that the fractal scaling of the stream chemistry may range over three orders of magnitude, even when rainfall chemistry appears as a white noise spectrum. Chen & Hsu (2007) evaluated the influence of the fractal geometry of porous media on groundwater flow and solute transport. Habib (2020) implemented fractal analysis to determine the long-term hydrological memory features. Sun *et al.* (2019) conducted a spectral analysis to determine the fractal dimensions of a groundwater system. Fractal analysis of a time series is based on quantifying the degree of fluctuation around the overall trend of the data over time. Such an approach can measure the complexity of a system and be adopted in this study.

Climate change may result in significant changes in the responses of hydrological systems in various areas of the world, including Taiwan. Guo *et al.* (2018) presented the frequency of extreme hydrological events and surface and groundwater changes in Taiwan owing to climate change. Hsu *et al.* (2007) quantitatively evaluated the impact of climate change on groundwater resources in the southern plains of Taiwan. Yeh *et al.* (2015) used the Mann–Kendall test to analyze the dynamics of streamflow data from 12 gauges, revealing a crucial decrease in the streamflow in Taiwan due to climate change, which endangers its surface water supply. Wang *et al.* (2020) indicated a possible remote connection in the hydrological response of island-scale subtropical and continental-scale frigid zones.

Similar to other areas of the world, Taiwan also encounters crises related to uncertain water resources due to climate change. For example, from late 2020 to June 2021, Taiwan experienced a severe water shortage because no single typhoon hit Taiwan in the expected typhoon season in 2020. Consequently, the country's reservoirs could not be replenished for the first time in 56 years. To conserve water, Taiwan stopped irrigating 24% of the total planted rice crop areas in 2021 (Lin & Syngle 2021). In addition, Taiwan recorded its hottest month in May of 2021; specifically, this was the hottest month since 1947. Thus, exploring the impact of climate change on hydrology is important for managing routine and emergency water resources.

Socioeconomically, mountainous watersheds have been shown to be important within the context of providing water and hydroelectricity. However, the current understanding of the hydrologic response to climate change is limited, and this is largely due to a scarcity of the necessary data. Therefore, this study aims to (1) explore the impacts of climate change on watershed hydrology and (2) perform hydrological analyses using an integrated approach for data-scarce watersheds. To the best of our knowledge, this is the first study to characterize and predict the hydrological response to climate change in a mountainous watershed in Taiwan. These results will provide an understanding of the distribution of water components under climate change; such insights are valuable within the context of water resource management. In addition, the proposed approach can be applied to data-scarce watersheds around the world to measure the impact of climate change on future water scarcity. The remainder of the paper is structured as follows: the methodology section describes methods tied to the use of physics-based hydrological, groundwater, and general circulation models (GCMs). In addition, spectrum analysis is introduced, and the power spectral exponent is described; the study site section provides information on the Wuling Mountain Watershed. The hydrological data are described in the following section. In the Results and Discussion section, the integrated approach is applied to the Wuling Mountain Watershed. The results of the SWAT with modular three-dimensional groundwater flow (SWAT-MODFLOW) modeling, spectrum analysis, and hydrological simulations are presented. Power spectral exponents are calculated for hydrological components of the future scenario and compared to those of the baseline period. The impact of climate change on the hydrological response of the Wuling Mountain Watershed and its implications for future water resources are discussed. Additionally, the limitations and assumptions of the study are discussed. Finally, the study is concluded.

## METHODOLOGY

### Physics-based model of SWAT-MODFLOW

SWAT-MODFLOW simulates the surface water–groundwater interactions by integrating the SWAT with the modular three-dimensional groundwater flow model (MODFLOW) (Kim *et al.* 2008; Jafari *et al.* 2021). SWAT simulates the hydrological processes and solute transport above the aquifer, whereas the MODFLOW models the groundwater flow in an aquifer (Park *et al.* 2019). The recharge calculated by SWAT serves as the upper boundary of the MODFLOW for the simulation of the groundwater flow in aquifers.

SWAT was developed by the Agricultural Research Service of the United States Department of Agriculture to simulate the water, sediment, and nutrient cycles in a watershed. SWAT was originally designed to estimate the impact of various agricultural management systems on watershed responses and is widely used for hydrological modeling (Bieger *et al.* 2017). SWAT simulates hydrologic processes through a lumped approach. The water balance is calculated to include various water components, as shown in Equation (1):

$$SW_t = SW_0 + \sum_{i=1}^t (R_{\text{day}}^i - Q_{\text{surf}}^i - E_a^i - \text{Perco}^i - Q_{\text{lat}}^i - Q_{\text{gw}}^i) \quad (1)$$

where  $SW_t$  is the final soil water content;  $SW_0$  is the initial water content;  $R_{\text{day}}^i$  is the rainfall on day  $i$ ;  $Q_{\text{surf}}^i$  is the surface runoff on day  $i$ ;  $E_a^i$  is the evapotranspiration on day  $i$ ;  $\text{Perco}^i$  is the percolation on day  $i$ ;  $Q_{\text{lat}}^i$  is the lateral flow on day  $i$  (through the soil profile); and  $Q_{\text{gw}}^i$  is the base flow on day  $i$  (groundwater recharge to stream). The SWAT model estimates the direct runoff volumes from given rainfall events using the soil conservation service-curve number (SCS-CN) method (USDA 1972). Erosion and sediment transport are calculated using the modified universal soil loss equation (Williams & Berndt 1977). In SWAT, a complex basin is divided into sub-basins and further disaggregated into smaller hydrologic response units (HRUs) to reflect the hydrological differences in land uses/covers, crops, soils, etc. Runoff is predicted for each sub-area and routed to obtain the total runoff for a basin. This improves accuracy and provides a better physical characterization of the water balance. A concise description of the distinct water balance components and their interactions in the SWAT can be found in Neitsch *et al.* (2009).

The MODFLOW groundwater flow numerical model (McDonald & Harbaugh 1988) is one of the most widely used groundwater models. It can be used to simulate a multi-layer aquifer system in steady, transient, confined, or unconfined aquifers. Within the groundwater system, MODFLOW can simulate external disturbances, including pumping, regional replenishment, evaporative dispersion, water level changes, and regional drainage.

Before the MODFLOW simulation, the modeling domain is discretized using grids. Based on the hydrogeological characteristics of each grid element, the aquifers can be homogeneous, heterogeneous, isotropic, or anisotropic. The head of the grid is calculated according to the groundwater flow equation and adjacent grids. The grid can then be categorized into three attributes: a variable head grid, a fixed head grid, and an invalid grid. Invalid grids are not included in the calculation. The groundwater flow equation that incorporates the momentum balance is in the following equation:

$$\frac{\partial}{\partial x} \left( K_{xx} \frac{\partial h}{\partial x} \right) + \frac{\partial}{\partial y} \left( K_{yy} \frac{\partial h}{\partial y} \right) + \frac{\partial}{\partial z} \left( K_{zz} \frac{\partial h}{\partial z} \right) + \varepsilon = S \frac{\partial h}{\partial t} \quad (2)$$

where  $S$  is the storage coefficient;  $\varepsilon$  is the sink/source term;  $K_{ii}$  is a component of the hydraulic conductivity tensor  $K$ , assuming that the principal direction follows the flow path, and  $h$  is the hydraulic head of the aquifer. Prescribed head, prescribed flux and mixed boundaries can be assigned to the boundary grids.

SWAT and MODFLOW are integrated as SWAT-MODFLOW. In SWAT, the smallest calculation HRU is a unique combination of land use/cover, soil, and slope and does not have a designated geographic location. Therefore, HRUs are disaggregated into individual polygons with specific geographic locations. These disaggregated HRUs are then intersected with the grid cells in MODFLOW to share common variables for SWAT and MODFLOW modeling. In MODFLOW, the river used to estimate the volumetric flow exchange rates between the aquifer and stream is intersected with the sub-basins in SWAT to transfer the groundwater return flow rates to the corresponding sub-basin stream.

Model performance is evaluated by three criteria. The Nash–Sutcliffe model efficiency coefficient (NSE) is used to assess the predictive skill of hydrological models and is defined in the following equation:

$$\text{NSE} = 1 - \frac{\sum_{i=1}^N (y_i - x_i)^2}{\sum_{i=1}^N (y_i - \bar{x})^2} \quad (3)$$

where  $x_i$  is the measured value;  $y_i$  is the simulated value;  $\bar{x}$  is the average of the measured values, and  $N$  represents the amount of data. A larger NSE value indicates a more precise simulation of the model.  $R$ -squared ( $R^2$ ) is a statistical measure that represents the proportion of the variance for a dependent variable that is explained by an independent variable or variables in a regression model. This can be defined as in the following equation:

$$R^2 = \frac{\sum_{i=1}^N (y_i - \bar{y})^2}{\sum_{i=1}^N (x_i - \bar{x})^2} \quad (4)$$

An  $R^2$  value close to 1 indicates a good model fit. Root-mean-square error (RMSE) is frequently used to measure the differences between values predicted by a model or estimator and the observed or experimental values. RMSE is defined as in the following equation:

$$\text{RMSE} = \sqrt{\frac{\sum_{i=1}^N (y_i - \bar{y})^2}{N}} \quad (5)$$

A smaller RMSE indicates a closer difference between an observation and an estimation.

Moriasi *et al.* (2007) and Parajuli *et al.* (2009) provided the following criteria for model performance: very good performance:  $0.75 < \text{NSE} \leq 1$  and  $0.9 \leq R^2 \leq 1$ ; good performance:  $0.65 < \text{NSE} \leq 0.75$  and  $0.75 \leq R^2 \leq 0.89$ ; and satisfactory performance:  $0.5 < \text{NSE} \leq 0.675$  and  $0.5 \leq R^2 \leq 0.74$ . A lower RMSE value indicates better performance of the model. The SWAT-MODFLOW has been successfully applied to investigate the surface water–groundwater interaction of an irrigated alluvial fan in central Taiwan (Ke 2014).

### Weather generation under climate change scenarios

The latest version of the statistically downscaled projections obtained from the Taiwan Climate Change Projection Information and Adaptation Knowledge Platform (TCCIP; <https://tccip.ncdr.nat.gov.tw/>) provides 5 km by 5 km grid-based projections for precipitation and temperature based on the CMIP5 (the fifth phase of the Coupled Model Intercomparison Project). The CMIP6 version of statistically downscaled projections is expected to be released in early 2023. The CMIP5 experiments were conducted using several GCMs under four representative concentration pathways (RCPs) of greenhouse gas emissions (i.e., RCP2.6, RCP4.5, RCP6.0, and RCP8.5) (IPCC 2013). The baseline period used to investigate the impact of climate change is from 1986 to 2005, and the future period is from 2021 to 2040 (WRA 2016). Based on the down-scaled information, 200 years of precipitation and temperature data were generated under various climate change scenarios. The methods used for weather generation are as follows:

Precipitation generation is composed of the following steps: (1) simulate the occurrence of wet and dry days using the Markov chain process and (2) generate the rainfall amount for wet days using a specific probability distribution. In Step 1, a first-order, two-state Markov chain was applied to describe the transitions of a system state according to the transition probability matrix. The model assumes that there are only two possible system states (i.e., wet and dry), where the current system state depends on the last system state. Each element of the transition probability matrix can be derived based on the observed daily rainfall data. Due to seasonal features, the matrix for each month was calculated. For example,  $P_m(w)$  is the probability of a wet day in a month  $m$  and  $P_m(w/w)$  and  $P_m(w/d)$  are the conditional probabilities of a wet day when the previous days are



wet and dry days, respectively, in month  $m$ . A uniform random variable  $x$  between 0 and 1 is employed to assign the state of the first day. When the variable  $x$  is less than or equal to  $P_m(w)$ , the system state is defined as a wet day; otherwise, the system state is defined as a dry day. The system states of days are assigned based on a transition probability matrix. For example, if the state of the previous day was wet, the current day will be generated as a wet day when the random variable  $x$  is less than or equal to  $P_m(w/w)$ ; otherwise, the current day is simulated to be a dry day. In Step 2, after deciding the system state using the Markov chain, the rainfall amount was sequentially generated based on a specific probability distribution. Several probability distributions are applicable when generating the daily rainfall amount, including exponential (Tung & Haith 1995), Weibull (Yu & Polycarpou 2002), two-parameter gamma (Corte-Real *et al.* 1999), and mixed exponential (Woolhiser & Roldan 1986) distributions. Among these probability distributions, the Weibull distribution appropriately approximates the daily rainfall in Taiwan (Yu *et al.* 2002). It produces reasonable mean and standard deviation values for rainfall. Thus, a Weibull distribution was adopted in this study to generate the rainfall amount. The mean and variance of the observed daily rainfall data were calculated for each month to obtain the Weibull distribution parameter. Subsequently, a cumulative distribution function for the Weibull distribution was linked with a uniform random variable  $x$  to generate the amount of rainfall on a wet day.

The rainfall generation model can further process downscaled projections to generate rainfall data for various climate change scenarios. For example, the mean of the observed daily rainfall can be adjusted (e.g.,  $-10\%$ ) according to the downscaled projections. However, the remaining rainfall characteristics (dry/wet status and variance) are assumed to be identical to the observed rainfall.

The daily temperature for each month is generated using a first-order autoregressive model as in the following equation:

$$T_k = \mu_m + \rho_{1m}(T_{k-1} - \mu_m) + \sqrt{1 - \rho_{1m}^2} \sigma_m v_k + \Delta\mu_m - \rho_{1m}\mu_m \quad (6)$$

where  $T_K$  is the temperature ( $^{\circ}\text{C}$ ) on day  $k$ ;  $\mu_m$  is the mean temperature ( $^{\circ}\text{C}$ ) in month  $m$ ;  $\sigma_m$  is the standard deviation of the daily temperature ( $^{\circ}\text{C}$ ) in month  $m$ ;  $\rho_{1m}$  is the lag-1 autocorrelation coefficient of the daily temperature in month  $m$ ;  $v_k$  is the random standard normal variate; and  $\Delta\mu_m$  is the change in the mean temperature ( $^{\circ}\text{C}$ ) in month  $m$  for the climate change scenarios. Using parameters  $\mu_m$ ,  $\sigma_m$ ,  $\rho_{1m}$ , and  $\Delta\mu_m$ , the daily temperature data in month  $m$  can be generated using the model.

### Spectrum analysis

Spectrum analysis is a useful tool for feature characterization of time series data (Kay & Marple 1981). It provides information about the dominant cycle during a period of a time series. For a continuous time function  $x(t)$ , which is represented as complex-valued and integrable, the signal energy  $S$  is defined in the following equation:

$$S = \int_{-\infty}^{\infty} |x(t)|^2 dt < \infty \quad (7)$$

Then, the continuous Fourier transform  $X(f)$  of  $x(t)$  exists and can be given by the following equation:

$$X(f) = \int_{-\infty}^{\infty} x(t) e^{-i2\pi ft} dt \quad (8)$$

The squared modulus of the Fourier transform defines the energy spectrum density (ESD) for a finite time interval or the power spectrum density (PSD) (or simply a power spectrum) for an infinite time interval  $S(f)$  of  $x(t)$ :

$$S(f) = |X(f)|^2 \quad (9)$$

The ESD and PSD represent the energy distribution as a function of frequency. Using Parseval's energy theorem (Bracewell 2000), Equation (7) can be expressed as the following:

$$\int_{-\infty}^{\infty} |x(t)|^2 dt = \int_{-\infty}^{\infty} |X(f)|^2 df \quad (10)$$

Equation (10) shows that the energy of the time-domain signal is equal to the energy of the frequency-domain transform,  $\int_{-\infty}^{\infty} S(f)df$ .

The spectrum density of a time series  $S(f)$  may exhibit fractal behavior and can be approximated to follow a power law spectrum as in the following equation:

$$S(f) = f^{-\beta} \quad (11)$$

The slope of  $S$  with respect to  $1/f$  on the Bode plot (log-log plot) provides the power spectral exponent  $\beta$  as in the following equation:

$$\beta = -\frac{\log(S)}{\log(f)} \quad (12)$$

$\beta$  describes the shape complex of an object and provides a statistical index of complexity, which compares the changes in patterns with their measurement scale (Malamud & Turcotte 1999). When  $\beta > 1$ , the time series is nonstationary with strong persistence. When  $1 > \beta > 0$ , the time series is stationary and weakly persistent. When  $\beta = 0$ , the time series is uncorrelated. When  $\beta < 0$ , the time series is stationary and exhibits antipersistence behavior.

## STUDY SITE

The Wuling catchment is in central Taiwan, as shown in Figure 1. The catchment is the headwater of the Hehuan River, which flows out of the catchment from the north side of the gap and flows into the Dajia River via the Nanhu River. The Dajia River not only significantly contributes water resources to irrigate central Taiwan, but it also provides up to approximately 40% of Taiwan's hydroelectric power. The Wuling catchment is characterized as an alpine tundra ecosystem with an area of approximately 1.52 km<sup>2</sup> and an elevation of more than 3,000 m altitude above mean sea level (AMSL). Forest and grassland cover 72 and 20% of the area, respectively. The remaining areas are low-density residential areas. The catchment is surrounded by the Hehuan Main Mountain (3,417 m AMSL), the Hehuan East Mountain (3,421 m AMSL), and the Hehuan Peak Mountain (3,217 m AMSL). The bowl-shaped catchment has a slope of approximately 14.94°, which is higher in its eastern portion and lower on the west side with a slope facing west. The Wuling Watershed is composed of dark gray, black argillite, slate, phyllite, and dark gray sandstone interbedding, referred to as the Miocene Lushan Formation. The average annual rainfall is 2,797 mm. The wet season is from April to September and the dry season is from October to March.

## HYDROLOGICAL DATA

The Wuling hydrological station is located at a latitude of 24°08'14"N and a longitude of 121°16'46"E, at an altitude of 3,087 m. Hourly meteorological and hydrological data, including precipitation, temperature, relative humidity, and streamflow, were collected from 14 March 2013 to 22 July 2015. Two cluster wells (DHW-06) (121°16'54", 24°08'35") are at an elevation of 3,023 m. The daily groundwater levels were measured and recorded. The two wells are 3 m apart. The shallow well is 20 m below the ground surface (BGS) and the deep well is 100 m BGS. The deep and shallow wells have diameters of 2 and 6 inches, respectively. The screening depth of the well is 5–17 m BGS for the shallow well, while there are two screens located at 61–67 and 88–94 m BGS for the deep well.

For consistency with the daily-based GCM model, all hourly data were transformed into daily data. The time series of the streamflow, precipitation, relative humidity, highest and lowest temperatures, and groundwater level are shown in Figure 2(a)–2(d). Figure 2(a) shows the high correlation and synchronization of the changes in precipitation and streamflow. Figure 2(b) shows similar variations but with a time lag between the relative humidity and precipitation. The highest and lowest temperatures exhibited daily and seasonal fluctuations, as shown in Figure 2(c). The highest and lowest temperatures are 19.96 and −16.83 °C, which occurred on 7 July 2014 and 23 January 2014, respectively. The largest temperature difference of 26.35 °C occurred on 31 January 2014. Low temperatures, those below 0 °C, occur during the winter. Figure 2(d) shows the groundwater levels and precipitation. The fluctuation of the groundwater level in the shallow well is normally greater than that of the deep well, which has a slightly delayed response. Occasionally, the groundwater level of the deep well may exceed that of the shallow well. According to the drill cores, debris accumulation is located at 0.0–0.5 m BGS and the following rock plate is dominated by phyllite with poor water permeability. The rock is integrated, and the cleavage is

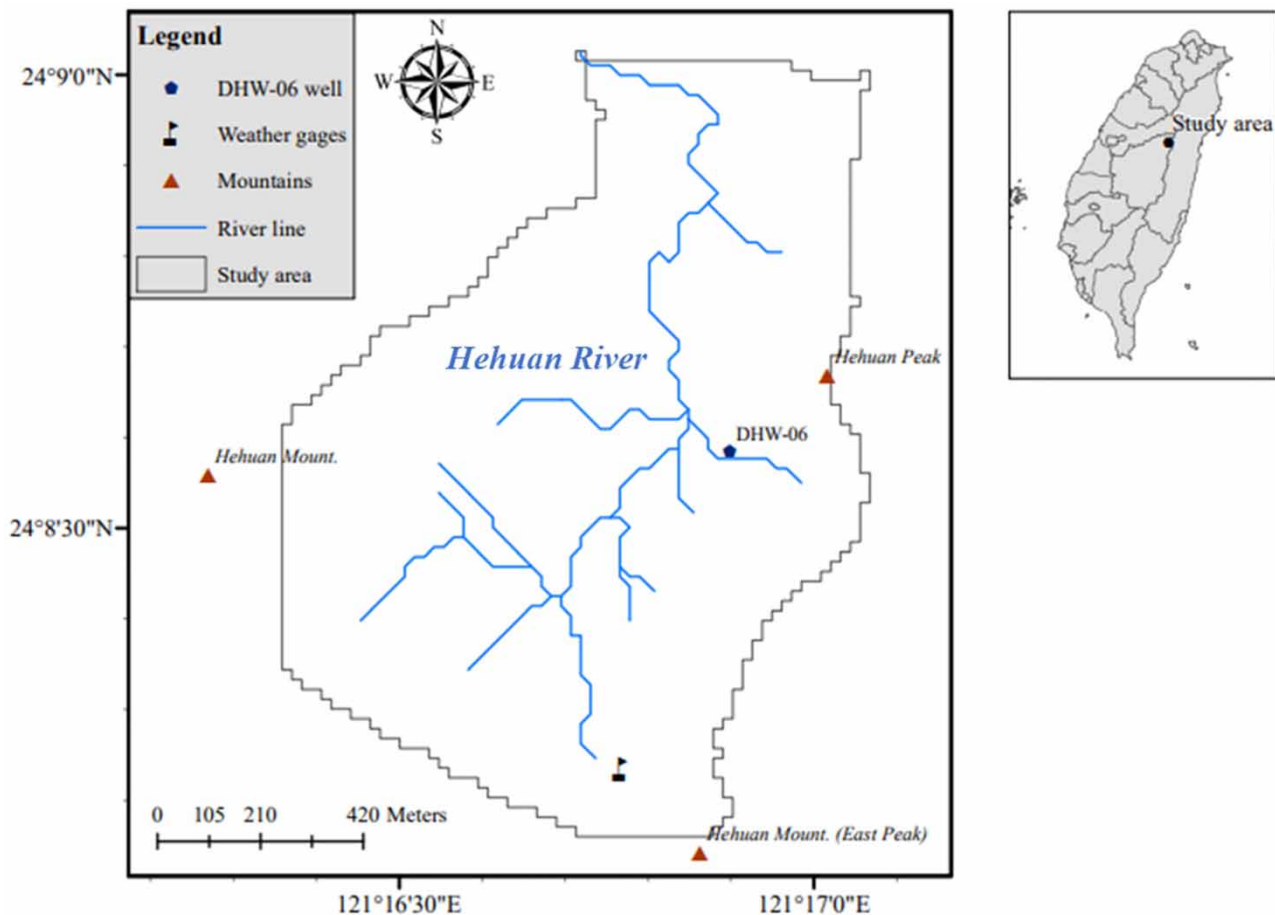


**Figure 1** | Map of the Wuling Watershed.

well-developed. Slight leakage was observed only at approximately 60–64 m BGS and 89 m BGS, which were below the shallow well. This may indicate that the deep and shallow wells are not in the same aquifer, which supports the possibility of the existence of a low-permeable layer to separate the shallow and deep wells.

## RESULTS AND DISCUSSION

### Hydrological responses during the observation period

The hydrological model was calibrated and validated using the SWAT-MODFLOW modeling. A total of 206 HRUs were generated for SWAT. A single-layer aquifer was simulated for the MODFLOW assuming that the connection between the shallow and deep wells is weak. Precipitation was set as the upper boundary for the SWAT-MODFLOW. Daily streamflow and monthly average groundwater level were used for the model's calibration and validation. Calibration and validation were performed using data obtained from 14 March 2013 to 31 December 2014 and from 1 January 2015 to 31 July 2015, respectively.

The input parameters of SWAT were processed and constrained within realistic uncertainty ranges based on the observed streamflow data. A sensitivity analysis was performed to identify the most sensitive parameters. In this study, 200 simulations were used for the sensitivity analysis. The sensitivities of the streamflow parameters are shown in Table 1. A small  $p$ -value indicates a lower probability of a nonzero regression coefficient. If the probability ( $p$ -value) is less than the significant value (0.05) of  $\alpha$ , the null hypothesis is rejected, indicating that the results are statistically significant. Table 1 shows that the parameter most sensitive to streamflow is the runoff curve number, followed by the soil-saturated hydraulic conductivity and the soil evaporation compensation factor. The results indicated that geomorphology, soil properties, and temperature also affected the streamflow, but not significantly. MODFLOW was executed using the monthly data. Hydraulic conductivity was found to be the most sensitive parameter in groundwater modeling.



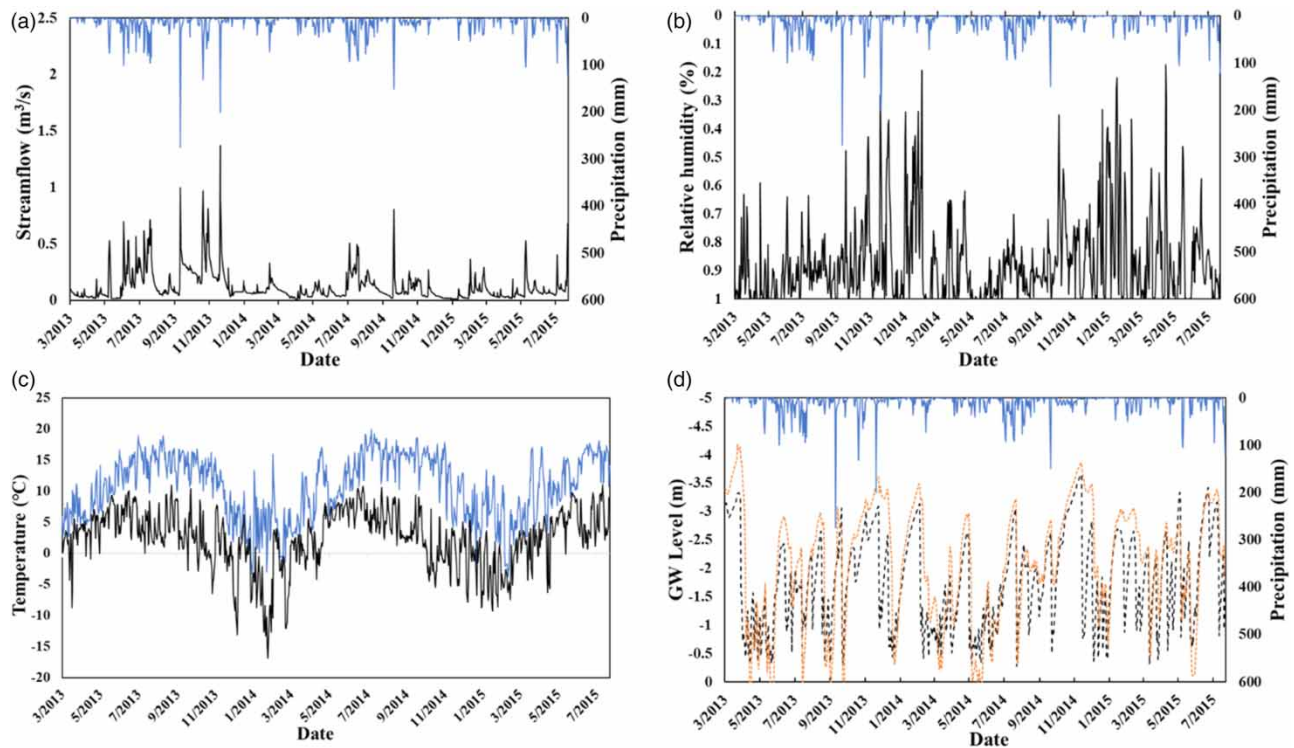


**Figure 2** | Time series of the (a) Precipitation (blue line) and streamflow (black line); (b) Precipitation (blue line) and relative humidity (black line); (c) Highest (blue line) and lowest (black line) temperature; and (d) Precipitation (blue line), shallow groundwater level (broken orange line), and deep groundwater level (broken black line). Please refer to the online version of this paper to see this figure in colour: <https://dx.doi.org/10.2166/wcc.2023.378>.

In this study, NSE and  $R^2$  were used to evaluate the results of the streamflow, whereas NSE,  $R^2$ , and the RMSE were used to evaluate the groundwater level. For the streamflow data, the calibration and validation had NSE values of 0.61 and 0.75, and  $R^2$  values of 0.77 and 0.8, respectively. For the groundwater level, the calibration and validation had NSE values of 0.85 and 0.8;  $R^2$  values of 0.765 and 0.65, and RMSE values of 0.41 and 0.44, respectively. Figure 3 shows the calibration and validation results for the variations in streamflow and groundwater level, confirming the proper use of the SWAT-MODFLOW model for the Wuling Mountain Watershed.

The water balance in the Wuling Watershed is presented in Table 2. Hydrological components, including the water yield, percolation, and evapotranspiration, were analyzed using 2-year data (1 July 2013–30 June 2015). The water yield represents the amount of water that leaves the watershed through reach, including the surface runoff, baseflow, and lateral flow (through the soil profile). The percentages of percolation, evapotranspiration, and water yield to precipitation were 10.94, 13.34, and

**Table 1** | Sensitivity of the parameters

| Ranking | Parameter | p-value              |
|---------|-----------|----------------------|
| 1       | CN2       | 0                    |
| 2       | SOL_K     | $2.6 \times 10^{-4}$ |
| 3       | ESCO      | $8.9 \times 10^{-4}$ |
| 4       | GW_DELAY  | $1.1 \times 10^{-3}$ |
| 5       | ALPHA_BF  | $1.2 \times 10^{-2}$ |
| 6       | SOL_AWC   | $4.9 \times 10^{-2}$ |

CN2 (–), runoff curve number, SOL\_K (mm/h), soil-saturated hydraulic conductivity, ESCO (–), soil evaporation compensation factor, GW\_DELAY (day), groundwater delay time, ALPHA\_BF (1/day), alpha factor for the groundwater recession curve of the deep aquifer, and SOL\_AWC (mm H<sub>2</sub>O/mm soil), available water capacity of the soil layer.

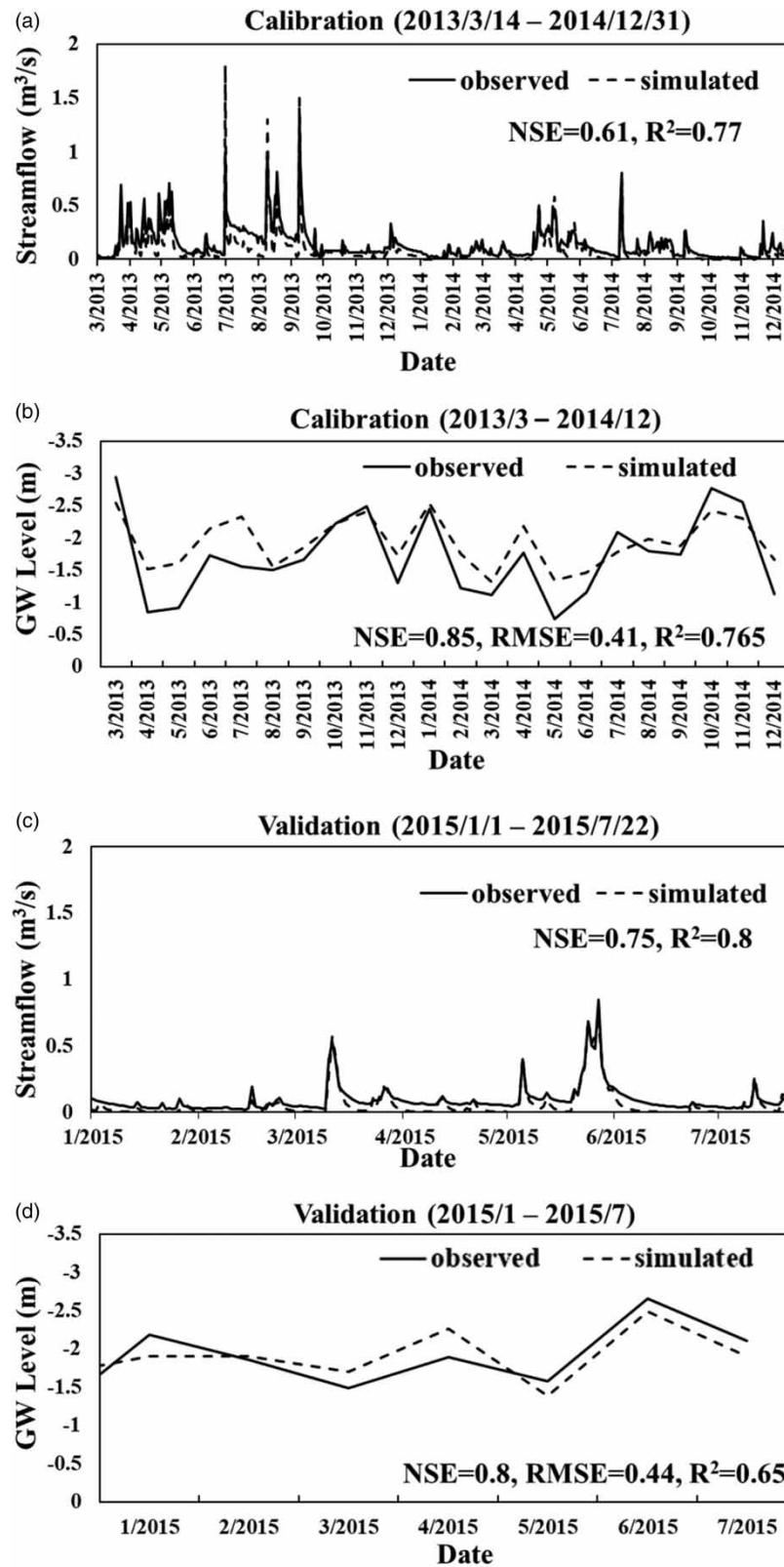


**Figure 3** | Model calibration and validation for variations in the streamflow and groundwater level.

**Table 2** | Water balance of the Wuling Watershed

| Water components (mm)    | 1 July 2013–30 June 2014 | 1 July 2014–30 June 2015 | Average  | Percentage of total water (%) |
|--------------------------|--------------------------|--------------------------|----------|-------------------------------|
| Precipitation            | 3,982.50                 | 2,798.50                 | 3,390.50 | 100.0                         |
| Percolation              | 407.25                   | 334.41                   | 370.83   | 10.94                         |
| Evapotranspiration       | 434.97                   | 469.83                   | 452.40   | 13.34                         |
| Water yield <sup>a</sup> | 3,140.28                 | 1,994.26                 | 2,567.27 | 75.72                         |

<sup>a</sup>Water yield includes streamflow, base flow, and lateral flow.

75.72%, respectively. Hence, three-fourths of the precipitation leaves the watershed through the reach, and approximately one-tenth of the total water percolates through the watershed. We observed that the year 2013 was wetter than usual and that the 2-year observation period (i.e., 2013–2015) was not long enough to comprehensively represent the weather in Wuling. Therefore, the 2-year observations were used to construct a 20-year baseline for the use of comparison with future projections.

### Hydrological responses of the baseline data

The baseline data are required as a reference to simulate future scenarios (2021–2040). The 1986–2005 precipitation data for the Wuling Watershed were reconstructed based on the nearby long-term stations (i.e., the Hehuan, Ya-Kao, Tsui, Cui-Feng, and Zing-Kuan stations) using the Normal Ratio method. Meanwhile, the 1986–2005 temperature data for the Wuling Watershed were reconstructed based on the nearest meteorological station (i.e., the Sun Moon Lake Station) using an elevation-based correction method, that is, a decrease of 0.6 °C for every 100 m increase in elevation.

The 1986–2005 temperature and precipitation data were applied to the calibrated SWAT-MODFLOW model and the water components were determined. Spectral analyses were applied to the hydrological time series and the power spectral exponents were calculated. Figure 4 shows the Bode plots of the hydrological components. Precipitation, stream flow, percolation, and evapotranspiration were weakly persistent, with small power spectral exponents of 0.1, 0.2, 0.18, and 0.1, respectively. In contrast, the temperature and groundwater level were mildly persistent with power spectral exponents of 0.7 and 0.85, respectively. The groundwater level exhibited strong damping from precipitation, whereas the other water components were closely linked to the precipitation.

The baseline water components were calculated using the SWAT-MODFLOW modeling. Figure 5 shows the monthly average baseline values of the water components. Monthly precipitation indicated a dry period from September to February and a wet period from March to August. The highest monthly precipitation was in May. The highest monthly temperature was recorded in July, while the lowest was in December. Evapotranspiration showed two peaks in March and June. The highest monthly percolation was in May and the lowest was in November. Streamflow was greatly sensitive to precipitation, with its highest and lowest values observed in May and November, respectively.

### Hydrological responses to projected climate scenarios

The RCPs form a set of greenhouse gas concentrations and emission pathways designed to support research on the impacts of and potential policy responses to climate change. The RCPs cover the range of the forcing levels associated with emission scenarios published in the literature. Four RCPs (i.e., 2.6, 4.5, 6.0, and 8.5) of the 21st-century pathways of greenhouse gas emissions, atmospheric concentrations, air pollution emissions, and land use were included in the Intergovernmental Panel on Climate Change (IPCC) fifth assessment report (AR5), as shown in Table 3. The downscaled precipitation and temperature projections under the RCP2.6, 4.5, 6.0, and 8.5 climate change scenarios were used to investigate the impact of climate change on major components of the hydrological cycle. Among the projections, RCP8.5 had the strongest driving forces for climate change.

By adopting future meteorological data, the hydrological components can be simulated for the near future scenario (2021–2040) using SWAT-MODFLOW. Changes in each water component were calculated and averaged. The results were compared to the baseline data (1986–2005). The results for the monthly changes in the water components with respect to the baseline data under the various RCP scenarios are shown in Figure 6. Positive and negative changes indicated increases and decreases in the water component values of the future scenario, respectively. Figure 6 shows a significant difference between the future and baseline data. Figure 6(a) shows a decrease in the precipitation during the dry season (October–March)

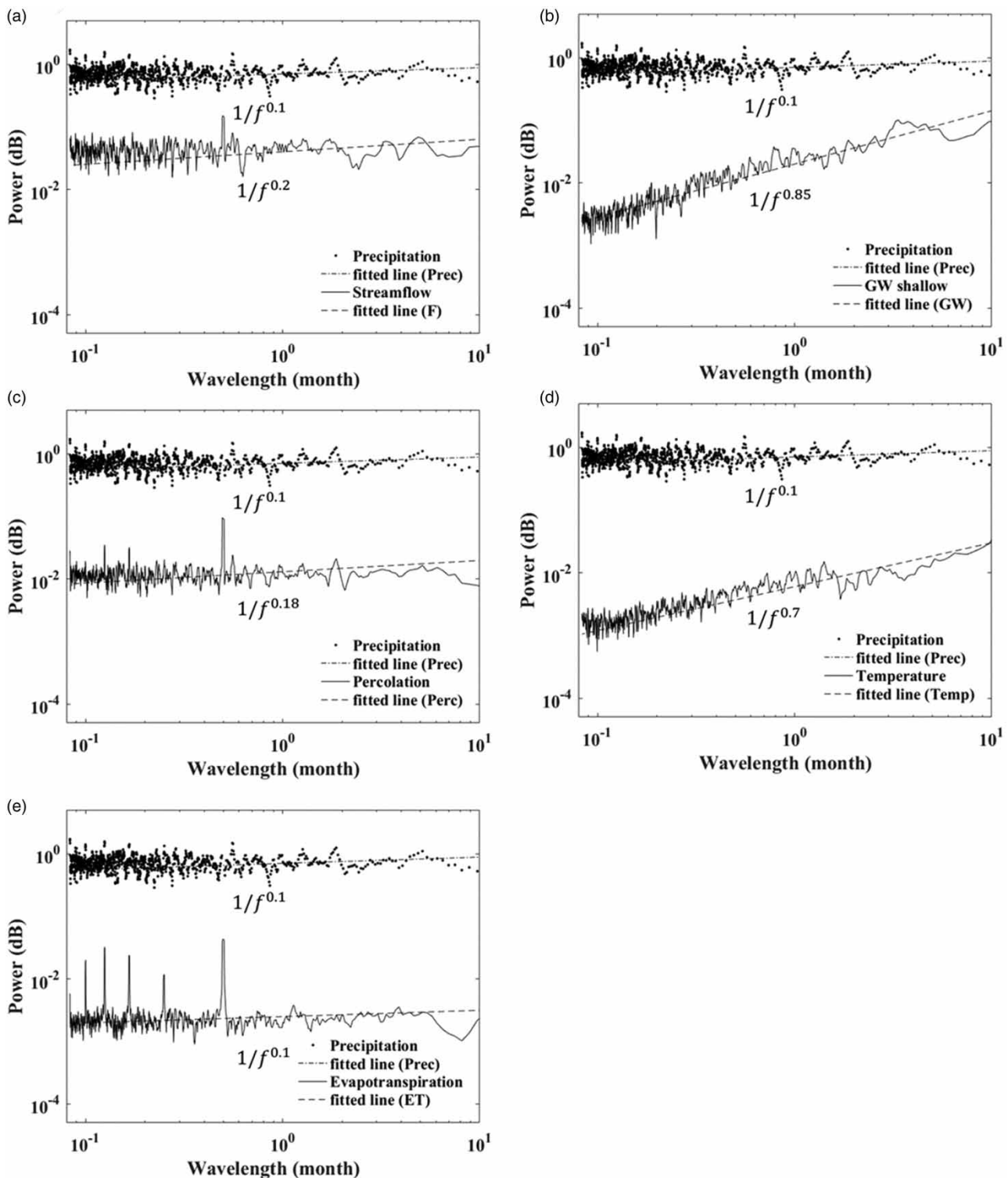


**Figure 4** | Spectra of the hydrological components for the baseline (1986–2005): (a) Streamflow; (b) Shallow groundwater level; (c) Percolation; (d) Temperature; and (e) Evapotranspiration. The dotted line shows the precipitation data.

and an increase in the precipitation during the wet season (April–September). The difference in these values was as high as from  $-10$  to  $20\%$ . [Figure 6\(b\)](#) shows that the monthly temperatures were higher than the baseline all year round and increased from  $0.1$  to  $1^\circ\text{C}$  for the projected period from 2021 to 2040. Changes in the percolation are shown in [Figure 6\(c\)](#)

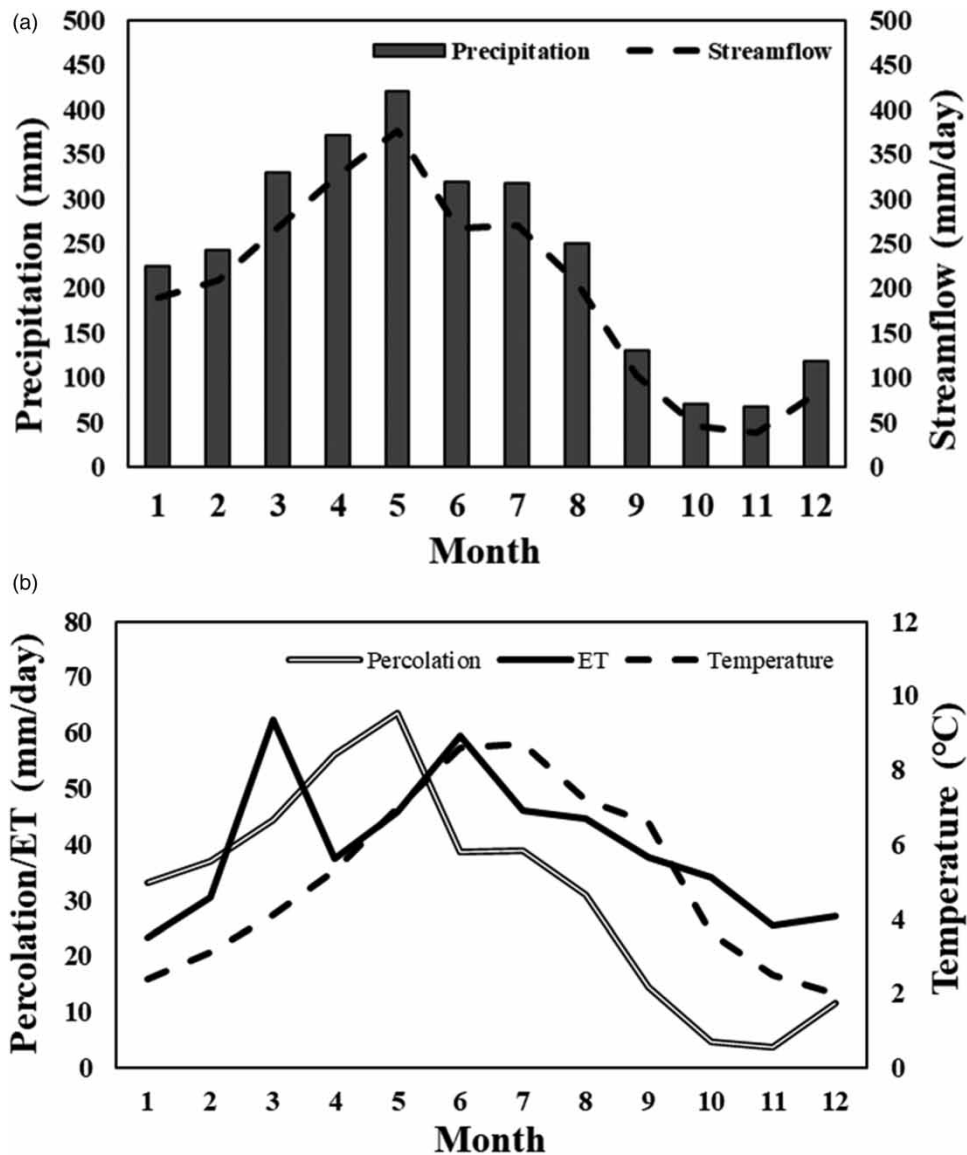


**Figure 5** | Baseline monthly average values (1986–2005) of (a) precipitation, streamflow, and, (b) percolation, temperature, and evapotranspiration (ET).

and follow the trend in the precipitation. In particular, the water percolation during the dry and wet seasons was lower by –10% and higher by 25%, respectively. Figure 6(d) shows the changes in evapotranspiration. The RCP scenarios had lower values than the baseline in January, March, and December, whereas they were higher than the baseline, by approximately 4%, for the other months. This may indicate faster hydrological cycling in the atmosphere. The changes in the

**Table 3** | Main characteristics of the RCPs used in the study

| Scenario component                         | RCP2.6           | RCP4.5                          | RCP6.0                          | RCP8.5 |
|--|------------------|---------------------------------|---------------------------------|--------|
| Radiative forcing ( $\text{W/m}^2$ )       | 2.6              | 4.5                             | 6.0                             | 8.5    |
| $\text{CO}_2$ equivalent (ppm)             | 490              | 650                             | 850                             | >1,370 |
| Pathway                                    | Peak and decline | Stabilization without overshoot | Stabilization without overshoot | Rising |
| Temperature anomaly ( $^{\circ}\text{C}$ ) | 1.5              | 2.4                             | 3.0                             | 4.9    |

Source: Wayne (2013).



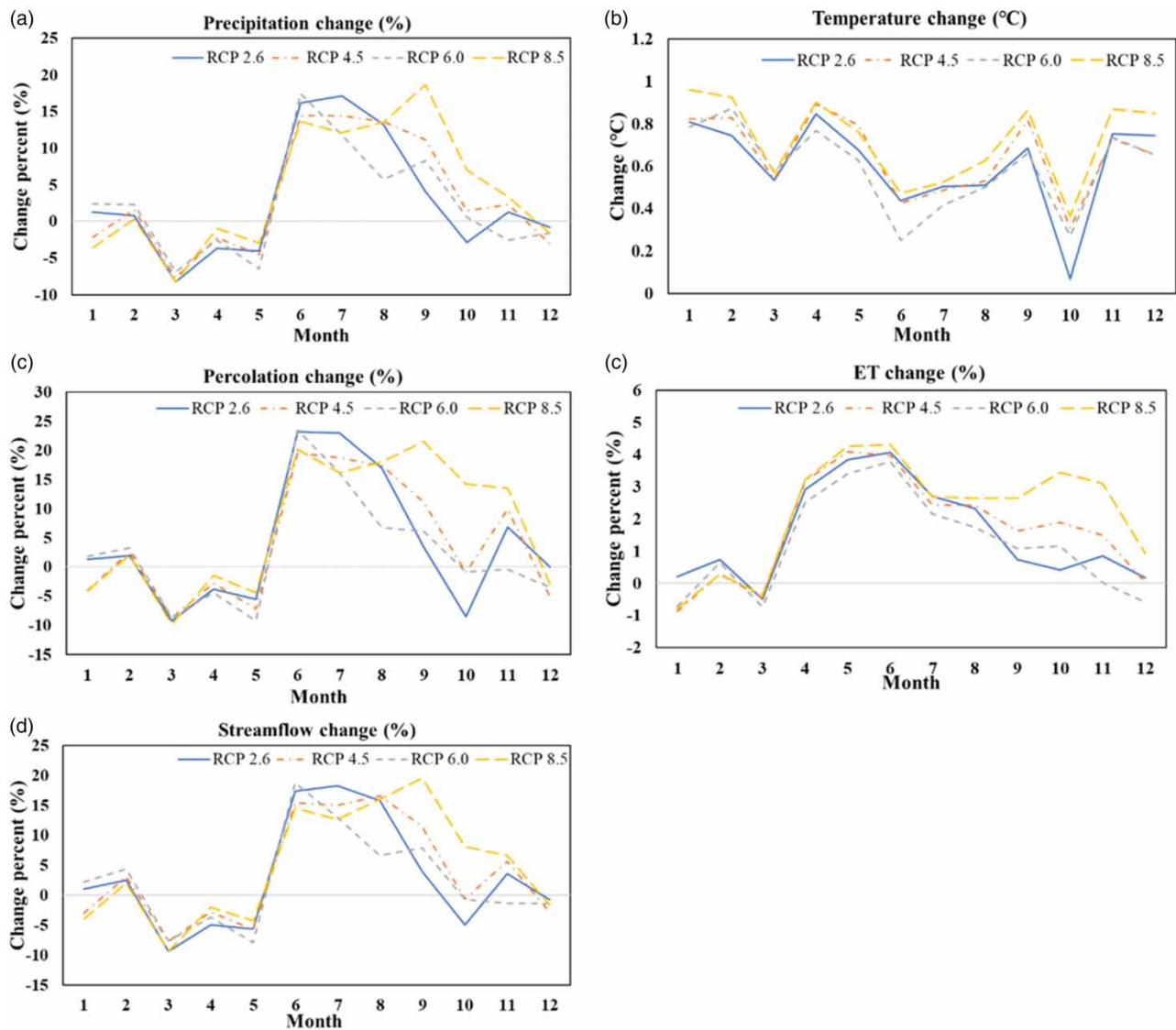


**Figure 6** | Comparison of the changes in the (a) Precipitation; (b) Temperature; (c) Percolation; (d) Evapotranspiration (ET); and (e) Streamflow under four RCP scenarios. Positive and negative changes indicate increases and decreases in the values, respectively.

streamflow closely follow those for the precipitation, as shown in Figure 6(e). Specifically, the changes in the streamflow during the dry and wet seasons were  $-10$  and  $20\%$ , respectively. Among the simulated RCP scenarios, RCP8.5 demonstrated the most significant deviations in different months; thus, RCP8.5 was adopted for the fractal analysis to represent the extreme case.

**Table 4** | A comparison of the baseline and future water compositions

| Water component (mm)     | Baseline projection |                               | Future projection |                               |
|--------------------------|---------------------|-------------------------------|-------------------|-------------------------------|
|                          | Average             | Percentage of total water (%) | Average           | Percentage of total water (%) |
| Precipitation            | 2,863.69            | 100.0                         | 3,151.83          | 100.0                         |
| Percolation              | 352.23              | 12.3                          | 387.68            | 12.3                          |
| Evapotranspiration       | 435.28              | 15.2                          | 450.71            | 14.3                          |
| Water yield <sup>a</sup> | 2,076.18            | 72.5                          | 2,313.44          | 73.4                          |

<sup>a</sup>Water yield includes streamflow, base flow, and lateral flow.

Climate change induces variation in the water distribution, as shown in Table 4. The future precipitation projection was approximately 10.1% higher than the baseline precipitation projection. For the baseline water cycle components in the Wuling Watershed, percolation, evapotranspiration, and water yield accounted for 12.3, 15.2, and 72.5% of the total

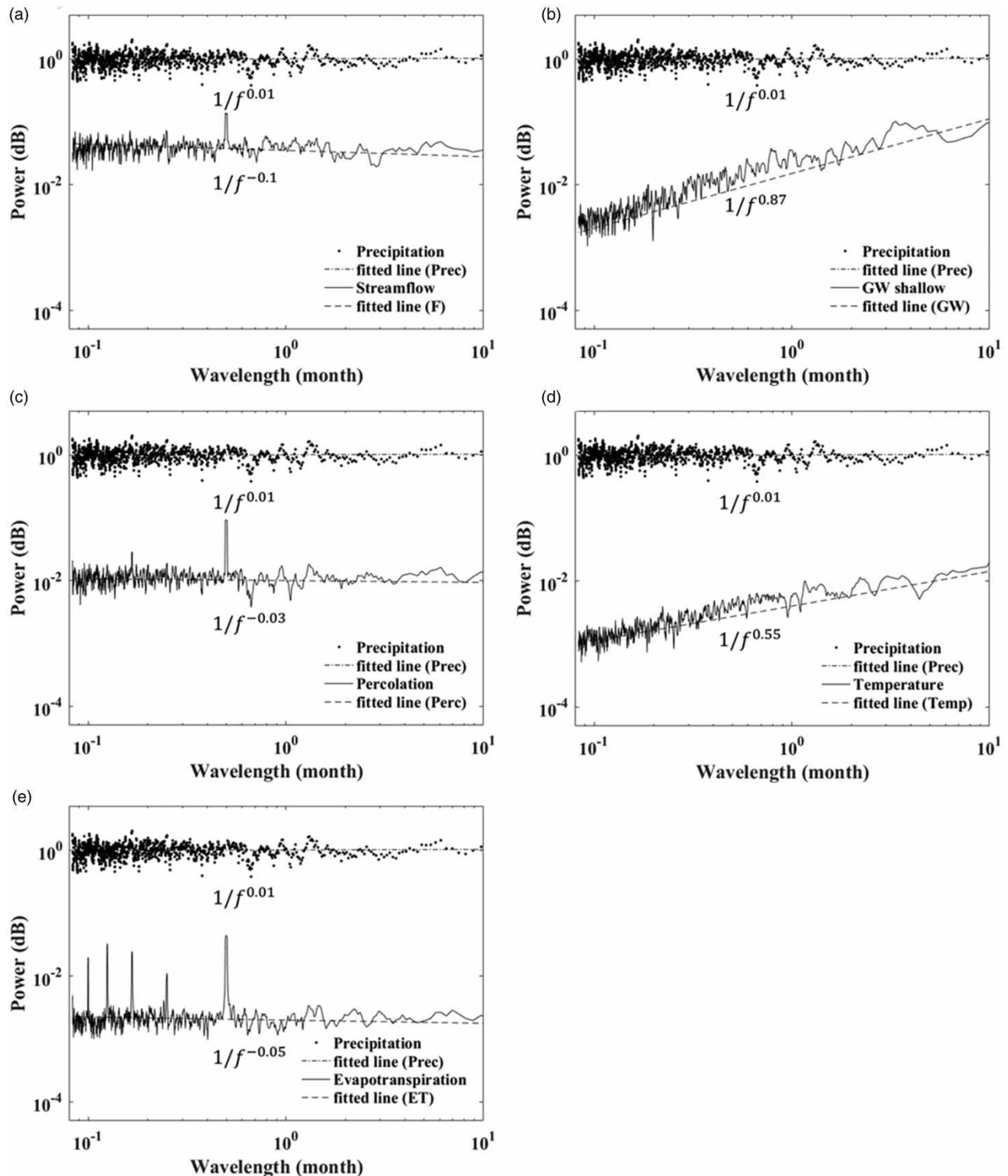


**Figure 7** | Spectra of the hydrological components for the future scenario (2021–2040): (a) Streamflow; (b) Shallow groundwater level; (c) Percolation; (d) Temperature; and (e) Evapotranspiration (ET). The dotted line shows the precipitation data.

water, respectively. For the future water cycle components, percolation, evapotranspiration, and water yield accounted for 12.3, 14.3, and 73.4% of the total water, respectively. The percentage of percolation components remained the same, whereas evapotranspiration and water yield decreased and increased, respectively. Besides the changes in water distribution, the annual amounts of the studied hydrological components all increase. The percolation, evapotranspiration, and water yield increased by 10.9, 3.3, and 11.3%, respectively. This indicates that the hydrological cycle accelerated and the water distribution changed in the hydrological components.

The Bode plots for the baseline and future projections are shown in Figures 4 and 7, respectively. The values of the power spectral exponent are shown in Table 5. The power spectral exponent of the precipitation changed from 0.10 of the baseline projection to 0.01 of the future projection. Precipitation tended toward white noise and was uncorrelated in the projected scenario. This increases the prediction difficulty. The power spectral exponent of the streamflow decreased from 0.20 to  $-0.10$ . The evapotranspiration and percolation exponents also decreased and changed from 0.10 to  $-0.05$  and from 0.18 to  $-0.03$ , respectively. These three water components changed from weak persistence to slight antipersistence. This suggests a statistically significant water discrepancy in neighboring years, indicating the increasing difficulty of surface water management in future scenarios. In contrast, the power spectral exponent of the groundwater level increased from 0.85 to 0.87 and remained mildly persistent. The groundwater exhibited damping and strong attenuation from precipitation, and thus, was more predictable.

### Implications for future water resources

Hydrological components are directly related to the available water resources. Our results showed that the hydrological components had different responses in the future projection as compared to the baseline projection. Precipitation increased in the wet seasons and decreased in the dry seasons under all RCP scenarios. The temperature has consistently increased throughout the year. Among the four RCP scenarios, RCP8.5 was the most drastic scenario, in which the changes in the percolation and streamflow corresponded highly to that of the precipitation. The lower streamflow in the dry season indicated less available surface water, while the higher streamflow in the wet season did not necessarily mean there was more surface water available. Instead, flood disasters and high-water turbidity could occur more frequently, and these conditions are not favorable within the context of water use. In particular, the amount of water increased in all water components and thus indicated an acceleration of the water cycle. In future climate projections, precipitation will tend toward white noise. Streamflow, evapotranspiration, and percolation became antipersistent, whereas the groundwater remained persistent. Thus, climate change significantly impacts surface water, while groundwater may serve as a buffer to mitigate the short-term impact on water resources, making groundwater fundamentally important for the water supply and other ecosystem-linked functions.

### Limitations and assumptions

In this study, we proposed an approach that integrated physics-based meteorological and hydrological models to characterize and predict changes in hydrological components caused by climate change for a data-scarce mountainous watershed. Data limitations and model assumptions were embedded in the proposed approach. First, to ensure consistency with the groundwater level data resolution, hydrological data were converted from hourly to daily. Therefore, extreme hydrological events such as peak flow were not modeled at short intervals. Nevertheless, this did not prevent the necessity of using spectral analysis to assess the impact of climate change on 10-day, monthly, and seasonal trends by comparing the power law exponents of two equal-length periods for time series from the baseline and future scenarios. In addition, land use, topography, and soil distribution were assumed to remain the same during the SWAT modeling period. The IPCC sixth assessment report

**Table 5** | Power spectral exponents  $\beta$  of the baseline and projected scenarios

| Water component    | Baseline | Projected scenario $\beta$ |
|--------------------|----------|----------------------------|
| Precipitation      | 0.10     | 0.01                       |
| Streamflow         | 0.20     | $-0.10$                    |
| Evapotranspiration | 0.10     | $-0.05$                    |
| Percolation        | 0.18     | $-0.03$                    |
| Groundwater level  | 0.85     | 0.87                       |

(AR6) can be used to further improve the modeling scenarios (IPCC 2022). Third, the slope effect on SWAT modeling is a concern (Bieger *et al.* 2015). Recent studies (Yacoub & Foguet 2013; Lu & Chiang 2019) have shown that SWAT is applicable for modeling mountainous watersheds (Yacoub & Foguet 2013; Lu & Chiang 2019). The denser HRUs help to delineate the hydrologic response to the topographic variation. In addition, the study site of the present study is small and has a mild topography, and the satisfactory calibration and verification results support the use of SWAT modeling.

## CONCLUSIONS

The short-term hydrological data, physics-based meteorological and hydrological models, and spectrum analysis were integrated to evaluate the hydrological response to climate change for a data-scarce watershed. The Wuling Mountain Watershed in central Taiwan was taken as the study site. Twenty-eight-month hydrological data from 2013 to 2015 were used for the hydrological characterization. The results showed that the combined use of the physics-based hydrological and GCM models provided a feasible approach for characterizing the hydrological component distribution under the climate change stress for data-scarce watersheds. This integrated approach can be applied to other data-scarce watersheds to measure the impact of climate change on future water scarcity. The results of scenarios from CMIP5 for the climate projection for the period 2021–2040 showed that the future precipitation, water percolation, and streamflow will decrease by about 10% and increase by about 20–25% in the dry and wet seasons, respectively. The evapotranspiration is lower than that of the baseline in January, March, and December, whereas it can be as high as 4% during the other months. Under the RCP8.5 scenario, annual amounts of all studied water components increase. Percolation, evapotranspiration, and water yield change from 12.3, 15.2, and 72.5% of the total water for the baseline to 12.3, 14.3, and 73.4%, respectively. The increase of the water amounts and changes of the water distribution indicate the possible acceleration of the water cycle. Spectrum analysis showed that surface water tends toward becoming more antipersistent and harder to predict, while groundwater remains mildly persistent. Thus, groundwater may serve as a buffer for the impact of climate change on water resources for the Wuling Mountain Watershed.

## ACKNOWLEDGEMENTS

This study was financially supported by the Ministry of Science and Technology of Taiwan under Grant No. MOST 111-2116-M-006-015 and MOST 111-2221-E-006-004. The data provided by the Central Geological Survey of Taiwan are greatly appreciated. The comments of the editor and two anonymous reviewers are greatly appreciated.

## DATA AVAILABILITY STATEMENT

All relevant data are included in the paper or its Supplementary Information.

## CONFLICT OF INTEREST

The authors declare there is no conflict.

## REFERENCES

- Afshar, A. A., Hasanzadeh, Y., Besalatpour, A. & Pourreza-Bilondi, M. 2017 Climate change forecasting in a mountainous data scarce watershed using CMIP5 models under representative concentration pathways. *Theoretical Applied Climatology* **129** (1), 683–699.
- Anaraki, M. V., Farzin, S., Mousavi, S.-F. & Karami, H. 2020 Uncertainty analysis of climate change impacts on flood frequency by using hybrid machine learning methods. *Water Resources Management* **35**, 199–223. <https://doi.org/10.1007/s11269-020-02719-w>.
- Bai, Z., Xu, Y.-P., Gu, H. & Pan, S. 2019 Joint multifractal spectrum analysis for characterizing the nonlinear relationship among hydrological variables. *Journal of Hydrology* **576**, 12–27.
- Balica, S., Popescu, I., Beevers, L. & Wright, N. G. 2013 Parametric and physically based modelling techniques for flood risk and vulnerability assessment: a comparison. *Environmental Modelling Software* **41**, 84–92.
- Bieger, K., Hörmann, G. & Fohrer, N. 2015 Detailed spatial analysis of SWAT-simulated surface runoff and sediment yield in a mountainous watershed in China. *Hydrological Sciences Journal* **60** (5), 784–800. doi:10.1080/02626667.2014.965172.
- Bieger, K., Arnold, J. G., Rathjens, H., White, M. J., Bosch, D. D., Allen, P. M., Volk, M. & Srinivasan, R. 2017 Introduction to SWAT+, a completely restructured version of the soil and water assessment tool. *JAWRA Journal of the American Water Resources Association* **53** (1), 115–130.



- Borah, D. & Bera, M. 2003 Watershed-scale hydrologic and nonpoint-source pollution models: review of mathematical bases. *Transactions of the ASAE* **46** (6), 1553.
- Bracewell, R. N. 2000 *The Fourier Transform and its Applications*, 3rd edn. McGraw-Hill, New York.
- Chen, K. C. & Hsu, K. C. 2007 A general fractal model of flow and solute transport in randomly heterogeneous porous media. *Water Resources Research* **43** (12), W12501. doi:10.1029/2007WR005934.
- Conoscenti, C., Angileri, S., Cappadonia, C., Rotigliano, E., Agnesi, V. & Märker, M. 2014 Gully erosion susceptibility assessment by means of GIS-based logistic regression: a case of Sicily (Italy). *Geomorphology* **204**, 399–411.
- Corte-Real, J., Xu, H. & Qian, B. 1999 A weather generator for obtaining daily precipitation scenarios based on circulation patterns. *Climate Research* **13** (1), 61–75.
- Farzin, S. & Anaraki, M. V. 2021 Modeling and predicting suspended sediment load under climate change conditions: a new hybridization strategy. *Journal of Water and Climate Change* **12** (6), 2422–2443.
- Farzin, S., Anaraki, M. V., Naeimi, M. & Zandifar, S. 2022 Prediction of groundwater table and drought analysis; a new hybridization strategy based on bi-directional long short-term model and the Harris hawk optimization algorithm. *Journal of Water and Climate Change* **13** (5), 2233–2254. doi:10.2166/wcc.2022.066.
- Guo, F. W., Wang, B. T., Hsu, K. C. & Dzhamalov, R. G. 2018 Study of changes in frequency of hydrological extreme for surface and ground water in Taiwan. *Taiwan Water Conservancy* **66** (4), 85–99.
- Habib, A. 2020 Exploring the physical interpretation of long-term memory in hydrology. *Stochastic Environmental Research Risk Assessment* **34** (12), 2083–2091.
- Hsu, K.-C., Wang, C.-H., Chen, K.-C., Chen, C.-T. & Ma, K.-W. 2007 Climate-induced hydrological impacts on the groundwater system of the Pingtung Plain, Taiwan. *Hydrogeology Journal* **15** (5), 903–913.
- Huang, Z. & Yang, H. 2015 Dominant climatic factor driving annual runoff change at catchments scale over China. *Hydrology Earth System Sciences Discussions* **12** (12), 12911–12945.
- Hurst, H. E. 1951 Long-term storage capacity of reservoirs. *Transactions of the American Society of Civil Engineers* **116** (1), 770–799.
- IPCC 2013 Climate change 2013: the physical science basis. In: *Contribution of Working Group I to the Fifth Assessment Report of the Intergovernmental Panel on Climate Change*. Cambridge University Press, Cambridge, UK; New York, NY, USA, p. 1535.
- IPCC 2022 Climate change 2022: impacts, adaptation & vulnerability. In: *Contribution of Working Group II to the Sixth Assessment Report of the Intergovernmental Panel on Climate Change*. Cambridge University Press in Press, Cambridge, UK; New York, NY, USA, p. 3675.
- Jafari, T., Kiem, A. S., Javadi, S., Nakamura, T. & Nishida, K. 2021 Fully integrated numerical simulation of surface water-groundwater interactions using SWAT-MODFLOW with an improved calibration tool. *Journal of Hydrology: Regional Studies* **35**, 100822.
- Kadkhodazadeh, M., Valikhan Anaraki, M., Morshed-Bozorgdel, A. & Farzin, S. 2022 A new methodology for reference evapotranspiration prediction and uncertainty analysis under climate change conditions based on machine learning, multi criteria decision making and Monte Carlo methods. *Sustainability* **14**, 2601. https://doi.org/10.3390/su14052601.
- Kay, S. M. & Marple, S. L. 1981 Spectrum analysis – a modern perspective. *Proceedings of the IEEE* **69** (11), 1380–1419.
- Ke, K.-Y. 2014 Application of an integrated surface water-groundwater model to multi-aquifers modeling in Choushui River alluvial fan, Taiwan. *Hydrological Processes* **28**, 1409–1421.
- Kim, N. W., Chung, I. M., Won, Y. S. & Arnold, J. G. 2008 Development and application of the integrated SWAT–MODFLOW model. *Journal of Hydrology* **356** (1–2), 1–16.
- Kirchner, J. W., Feng, X. & Neal, C. 2000 Fractal stream chemistry and its implications for contaminant transport in catchments. *Nature* **403** (6769), 524–527.
- Liang, W., Bai, D., Wang, F., Fu, B., Yan, J., Wang, S., Yang, Y., Long, D. & Feng, M. 2015 Quantifying the impacts of climate change and ecological restoration on streamflow changes based on a Budyko hydrological model in China's loess Plateau. *Water Resources Research* **51** (8), 6500–6519.
- Lin, O. & Syngle, E. 2021 *Taiwan Drought Results in Rice Area Reduction and Crop Loss*. Global Agricultural Information Network, Voluntary Report TW2021-0037.
- Liu, R., Liu, S. C., Shiu, C.-J., Li, J. & Zhang, Y. 2016 Trends of regional precipitation and their control mechanisms during 1979–2013. *Advances in Atmospheric Sciences* **33** (2), 164–174.
- Liu, W., Park, S., Bailey, R. T., Molina-Navarro, E., Andersen, H. E., Thodsen, H., Anders, N., Erik, J., Skødt, J. J., Birk, J. J. & Trolle, D. 2020 Quantifying the streamflow response to groundwater abstractions for irrigation or drinking water at the catchment scale using SWAT and SWATMODFLOW. *Environmental Sciences Europe* **32** (1), 1–25.
- López-Ortega, O., Pérez-Cortés, O., Castillejos-Fernández, H., Castro-Espinoza, F.-A. & González-Mendoza, M. 2020 Written documents analyzed as nature-inspired processes: persistence, anti-persistence, and random walks – we remember, as along came writing – T. Holopainen. *Applied Sciences* **10** (18), 6354.
- Lu, C.-M. & Chiang, L.-C. 2019 Assessment of sediment transport functions with the modified SWAT-Twn model for a Taiwanese small mountainous watershed. *Water* **11**, 1749. doi:10.3390/w11091749.
- Malamud, B. D. & Turcotte, D. L. 1999 Self-affine time series: measures of weak and strong persistence. *Journal of Statistical Planning Inference* **80** (1–2), 173–196.
- McDonald, M. G. & Harbaugh, A. W. 1988 *A Modular Three-Dimensional Finite-Difference Ground-Water-Flow Model*. U. S. Geological Survey Techniques of Water-Resources. Investigation, Book 6, Chap. A1 Reston, p. 586.



- Moriasi, D. N., Arnold, J. G., Van Liew, M. W., Bingner, R. L., Harmel, R. D. & Veith, T. L. 2007 [Model evaluation guidelines for systematic quantification of accuracy in watershed simulations](#). *Transactions of the ASABE* **50** (3), 885–900.
- Neitsch, S. L., Arnold, J. G., Kiniry, J. R. & Williams, J. R., 2009 1.1 Overview of soil and water assessment tool (SWAT) model. In: *Soil and Water Assessment Tool (SWAT): Global Application* (Arnold J., Srinivasan R., Neitsch S., George C., Abbaspour K., Gassman P., Fang H. H., Av G., Gosain A., Debels P., Kim N. W., Somura H., Ella V., Leon L., Jintrawet A., Reyes M. & Sombatpanit S., eds). World Association of Soil and Water Conservation, Bangkok.
- Parajuli, P. B., Nelson, N. O., Frees, L. D. & Mankin, K. R. 2009 [Comparison of AnnAGNPS and SWAT model simulation results in USDA-CEAP agricultural watersheds in south-central Kansas](#). *Hydrological Processes* **23** (5), 748–763.
- Park, S., Nielsen, A., Bailey, R. T., Trolle, D. & Bieger, K. 2019 [A QGIS-based graphical user interface for application and evaluation of SWAT-MODFLOW models](#). *Environmental Modelling Software* **111**, 493–497.
- Perrin, C., Michel, C. & Andréassian, V. 2003 [Improvement of a parsimonious model for streamflow simulation](#). *Journal of Hydrology* **279** (1–4), 275–289.
- Pourghasemi, H. R., Yousefi, S., Kornejady, A. & Cerdà, A. 2017 [Performance assessment of individual and ensemble data-mining techniques for gully erosion modeling](#). *Science of the Total Environment* **609**, 764–775.
- Sharma, A., Wasko, C. & Lettenmaier, D. P. 2018 [If precipitation extremes are increasing, why aren't floods?](#) *Water Resources Research* **54** (11), 8545–8551.
- Sivakumar, B., Berndtsson, R., 2010 Nonlinear dynamics and chaos in hydrology. In: *Advances in Data-Based Approaches for Hydrologic Modeling Forecasting* (Sivakumar, B. & Berndtsson, R., eds). World Scientific, Singapore, pp. 411–461.
- Solomatine, D. P. & Ostfeld, A. 2008 [Data-driven modelling: some past experiences and new approaches](#). *Journal of Hydroinformatics* **10** (1), 3–22.
- Sun, H., Gu, X., Zhu, J., Yu, Z. & Zhang, Y. 2019 [Fractal nature of groundwater level fluctuations affected by riparian zone vegetation water use and river stage variations](#). *Scientific Reports* **9** (1), 1–9.
- Taormina, R. & Chau, K.-W. 2015 [Data-driven input variable selection for rainfall-runoff modeling using binary-coded particle swarm optimization and Extreme Learning Machines](#). *Journal of Hydrology* **529**, 1617–1632.
- Tegegne, G., Park, D. K. & Kim, Y.-O. 2017 Comparison of hydrological models for the assessment of water resources in a data-scarce region, the Upper Blue Nile River Basin. *Journal of Hydrology: Regional Studies* **14**, 49–66.
- Tsegaw, A. T., Pontoppidan, M., Kristvik, E., Alfreðsen, K. & Muthanna, T. M. 2020 [Hydrological impacts of climate change on small ungauged catchments – results from a global climate model-regional climate model-hydrologic model chain](#). *Natural Hazards Earth System Sciences* **20** (8), 2133–2155.
- Tung, C.-P. & Haith, D. A. 1995 [Global-warming effects on New York streamflows](#). *Journal of Water Resources Planning Management* **121** (2), 216–225.
- US Soil Conservation Service 1972 *SCS National Engineering Handbook, Section 4: Hydrology*. Govt. Print. Off, Washington.
- Wang, B.-T., Grigorev, V. Y., Tseng, H.-W., Dzhamalov, R. G., Frolova, N. L., Yu, P.-S. & Hsu, K.-C. 2020 [The responses of precipitation and streamflow to recent climate variations in the frigid and subtropical zones](#). *Journal of Water Climate Change* **11** (1), 54–73.
- Water Resources Agency 2016 *Impact Assessment of Rainfall Variation Under Different Climate Change Scenarios on Flood and Drought (1/2)*. Project MOEAWRA1050215, Water Resources Agency, Ministry of Economic Affairs, Taiwan.
- Wayne, G. 2013 *The Beginner's Guide to Representative Concentration Pathways*. Skeptical Science, [http://www.skepticalscience.com/docs/RCP\\_Guide.pdf](http://www.skepticalscience.com/docs/RCP_Guide.pdf)
- Williams, J. & Berndt, H. 1977 [Sediment yield prediction based on watershed hydrology](#). *Transactions of the ASAE* **20** (6), 1100–1104.
- Woolhiser, D. A. & Roldan, J. 1986 [Seasonal and regional variability of parameters for stochastic daily precipitation models: South Dakota, USA](#). *Water Resources Research* **22** (6), 965–978.
- Yacoub, C. & Foguet, A. P. 2013 [Slope effects on SWAT modeling in a mountainous basin](#). *Journal of Hydrologic Engineering* **18** (12), 1663–1673.
- Yeh, C.-F., Wang, J., Yeh, H.-F. & Lee, C.-H. 2015 [Spatial and temporal streamflow trends in northern Taiwan](#). *Water* **7** (2), 634–651.
- Yu, N. & Polycarpou, A. A. 2002 [Contact of rough surfaces with asymmetric distribution of asperity heights](#). *Journal of Tribology* **124** (2), 367–376.
- Yu, P.-S., Yang, T.-C. & Wu, C.-K. 2002 [Impact of climate change on water resources in southern Taiwan](#). *Journal of Hydrology* **260** (1–4), 161–175.
- Zahabiyou, B., Goodarzi, M., Bavani, A. M. & Azamathulla, H. M. 2013 [Assessment of climate change impact on the Ghareh River Basin using SWAT hydrological model](#). *CLEAN – Soil, Air, Water* **41** (6), 601–609.
- Zheng, F., Maier, H. R., Wu, W., Dandy, G. C., Gupta, H. V. & Zhang, T. 2018 [On lack of robustness in hydrological model development due to absence of guidelines for selecting calibration and evaluation data: demonstration for data-driven models](#). *Water Resources Research* **54** (2), 1013–1030.
- Zhou, L., Meng, Y., Lu, C., Yin, S. & Ren, D. 2020 [A frequency-domain nonstationary multi-site rainfall generator for use in hydrological impact assessment](#). *Journal of Hydrology* **585**, 124770.

First received 27 September 2022; accepted in revised form 22 March 2023. Available online 6 April 2023